An Ultra-Broadband Terahertz Absorber at High Terahertz Frequency

Tong Li
Harbin Institute of Technology
Hang Chen
Harbin Institute of Technology
Fengqiang Zhang
Harbin Institute of Technology
Jia Zhang
Harbin Institute of Technology
Zhenlong Wang (wangzl@hit.edu.cn)
Harbin Institute of Technology

Research Article

Keywords: Terahertz, Broadband absorber, Metamaterials

Posted Date: February 8th, 2022

DOI: https://doi.org/10.21203/rs.3.rs-1190132/v1

An ultra-broadband terahertz absorber at high terahertz frequency

Tong Li,[1] Hang Chen,[1] Fengqiang Zhang, [3]Jia Zhang,[1, 2*] and Zhenlong Wang[1, 2*]

[1]*School of Mechatronics Engineering, Harbin Institute of Technology, Harbin 150001, China*

[2]*Key Laboratory of Microsystems and Microstructures Manufacturing, Ministry of Education, Harbin Institute of Technology, Harbin 150080, China*

[3]*School of Mechatronics Engineering and Automation, Harbin Institute of Technology, Shenzhen 518055, China*

[*]Corresponding Author: Jia Zhang and Zhenlong Wang

E-mail Address: zhangjia@hit.edu.cn (J. Z.); wangzl@hit.edu.cn

Abstract

Broadband absorber at high terahertz frequency is highly required for applications in imaging, detecting, electromagnetic stealth. Although intensive investigations of the broadband absorber have been taken, the challenges still exist both in design and fabrication of an ultra-broadband absorber at high frequency. Herein, a three-layered structure metamaterial has been designed to realize an ultra-broadband terahertz absorber covering 3.94-9.98 THz (6.04 THZ) at the absorption above 80%, and the absorption bandwidth can be increased to 7.64THz (2.34-9.98 THz) by rotating the absorber. Upon on the simulations, the proposed absorber exhibits insensitive to the TM and TE polarization, it means the absorption effect is almost consistent in different polarization modes, the proposed absorber is significant in the practical application. Nevertheless, the absorption bandwidth reduces a little bit to 5.05 THz (absorption >60%) as β increases to 45°.

Keywords: Terahertz; Broadband absorber; Metamaterials

1. Introduction

Terahertz wave is a kind of electromagnetic wave with a frequency range of 0.1-10 THz[1-3], which has many unique advantages of strong penetrability, high resolution and low photon energy[4-6]. It has great potential in imaging, nondestructive detection, spectrum analysis[7-9]. The discovery of electromagnetic metamaterials has provided a novel approach for preparation of terahertz absorbing material. Since the first experimental demonstration of a near-perfect microwave metamaterial absorber[10], the metamaterial terahertz absorber has received extensive attentions and researches[11-13]. However, most attempts are focused on the single absorption frequencies or narrow-band absorption [14-18]. Actually, the broadband absorber can absorb more electromagnetic waves, it is more important in the fields, such as electromagnetic stealth, terahertz imaging and sensing. In the last decade, many attempts of preparation of broadband absorbers have been made, however, the absorption bands are almost

in the low terahertz frequency (0.1-5 THz)[19-21]. There is still challenges for designing ultra-broadband absorber at the increased terahertz frequency[22-24].

In this letter, we proposed an ultra-broadband terahertz absorber which is a metamaterial with a three-layered structure. The absorber covers the high frequency terahertz regime of 3.94-9.98 THz at the absorption above 80%, and near entire terahertz regime at the absorption above 60%. The special designed ten nested aluminum rings with an opening structure will response for such an ultra-broadband absorption. Significantly, the proposed absorber exhibits insensitive to the TM and TE polarization no matter what kinds of incident angles are applied.

2. Structure and design

The proposed broadband absorber is a kind of periodic metamaterials, and the cell is schematically illustrated in Fig. 1. It contains three layers: a metallic bottom layer, another metallic top layer and a dielectric middle layer. The proposed metamaterial absorber is represented as "NROS" (nested rings with an opening structure) absorber.

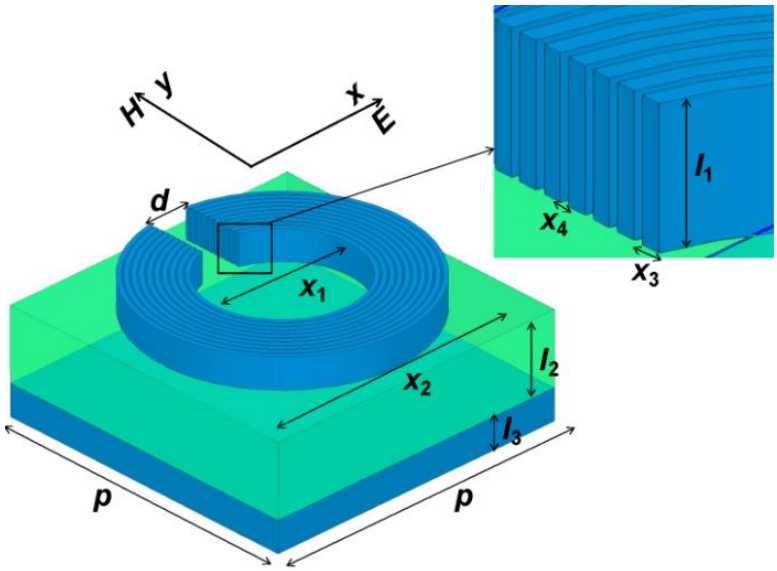

Fig. 1. 3D model of the cell of the proposed absorber. Enlarged view shows the nested rings of top layer. All structural parameters are marked with black symbol.

Specifically, the top layer is consisted of ten nested rings with an opening structure. The diameter of the innermost and outmost circle is represented as x_1 and x_2, while the width of each circle and inter distance of adjacent circles is recorded as x_3 and x_4, respectively. The width of opening structure is d, and the periodicity of the unit cell both in x and y directions is p. The

thickness of each layer from top to down is defined as l_1, l_2 and l_3, respectively. Based on the systematic simulations, the absorption can achieve maximum value when both the relative permittivity (ε_1) and permeability (μ_1) of metallic layer are about 1. Meanwhile, the ε_2 and μ_2 of middle dielectric layer should be about 2 and 1, respectively. Therefore, the aluminum metal is chosen for both of top and bottom layer, while polyethylene is selected to the middle dielectric layer with ε_2=2.25 and μ_2=1, respectively. All the design parameters are shown in Table 1.

Table1. Design parameters of proposed metamaterial absorber

Layer	Structure parameters	Materials	
		Name	Physical parameters
Top layer	d=5μm, x_1=14.4μm, x_2=26μm, x_3=0.4μm, x_4=0.2μm, l_1=0.02μm p=30μm	Aluminum	ε=1, μ=1
Dielectric layer	l_2=7μm	Polyimide	ε=3.5, μ=1
Bottom layer	l_3=1μm	Aluminum	ε=1, μ=1

The simulations of the periodic structure are carried out by employing finite difference time domain method based on "ANSYS Electronics 2017" soft. Absorption can be calculated by $A(\omega)=1-R(\omega)-T(\omega)$, $R(\omega)$ is reflectivity, $T(\omega)$ is transmissivity. S_{11} is reflection coefficient, S_{21} is transmission coefficient, $R(\omega)=|S_{11}|^2$, $T(\omega)=|S_{21}|^2$. According to the matrix transmission principle, the transmission matrix of electromagnetic wave in metamaterials can be calculated as:

$$T=\begin{pmatrix} \cos(nkh) & -\frac{z}{k}\sin(nkh) \\ \frac{k}{2}\sin(nkh) & \cos(nkh) \end{pmatrix} \quad (1)$$

In the Eq.1, n is refractive index of uniform tablet, k is wave vector of incident wave, h is thickness of uniform tablet, z is equivalent impedance of medium plate. The structure size of metamaterials is much smaller than the working wavelength, the metamaterials can be consider as homogeneous materials. S_{11} and S_{21} can be calculated as:

$$S_{11} = \frac{i}{2}\left(\frac{1}{z} - z\right)\sin(nkh) \tag{2}$$

$$S_{21} = \frac{1}{\cos(nkh) - \frac{i}{2}(z + \frac{1}{z})\sin(nkh)} \tag{3}$$

Eq.4 shows the relation of refractive index (n), impedance (z), permittivity (ε), and permeability (μ).

$$n = \varepsilon z = \frac{\mu}{z} \tag{4}$$

According to Eq. (2~4), we can deduce the relation between S_{11}, S_{21} and z, n, ε, μ (see Eq.5~8).

$$z = \sqrt{\frac{(1 + S_{11})^2 - S_{21}^2}{(1 - S_{11}^2) - S_{21}^2}} \tag{5}$$

$$n = \frac{1}{kh}\cos^{-1}[\frac{1}{2S_{21}}(1 - S_{11}^2 + S_{21}^2)] \tag{6}$$

$$\varepsilon = \frac{1}{kh}\cos^{-1}[\frac{1}{2S_{21}}(1 - S_{11}^2 + S_{21}^2)\sqrt{\frac{1 - S_{11}^2 - S_{21}^2}{(1 + S_{11})^2 - S_{21}^2}} \tag{7}$$

$$\mu = \frac{1}{kh}\cos^{-1}[\frac{1}{2S_{21}}(1 - S_{11}^2 + S_{21}^2)\sqrt{\frac{(1 + S_{11})^2 - S_{21}^2}{1 - S_{11}^2 - S_{21}^2}} \tag{8}$$

According to impedance matching principle, when equivalent impedance (z) is closer to the impedance of metamaterial interface with air, the reflectivity is lower. As Eq.4 shown, we can change the impedance (z) by controlling permittivity (ε). For the metamaterial absorber, the permittivity (ε) can be selected by controlling the size and geometry of periodic structure.

Different from the "CNR" (closed and nested rings) absorber, NROS absorber has an opening structure in the nested rings which makes a better absorption broadband. Fig. 2(a-d) are the current fields of CNR and NROS metamaterial absorber at their resonance frequency, the current fields are mainly distributed in the horizontal metal line of the closed nested metal ring in the resonant state, it means the horizontal metal line of the closed nested metal ring is equivalent to the inductance (L), the vertical metal line is equivalent to the capacitance (C) (see Fig. 2(f)). Fig.2 (f) is equivalent circuit of CNR and NROS metamaterial absorber, R in the

circuit is the equivalent resistance of energy loss. *L* and *C* are the equivalent inductance and capacitance of the metal patch structure. Whether NROS absorber or CNR absorber, each nested ring means a LC resonant circuit, there are 10 parallel LC resonant circuits in the equivalent circuit of CNR and NROS metamaterial absorber. When the metamaterial absorber is in perfect absorption, each *LC* resonance circuit can make an absorption curve, and the absorption curve is equivalent to the resonance curve, so the frequency of absorption peak is equal to the resonant frequency [see Eq. 9].

$$f = \frac{1}{T} = \frac{1}{2\pi\sqrt{LC}} \tag{9}$$

T is the oscillation period of LC resonance circuits, it also can be the bandwidth of absorption. There are ten LC resonance circuits, it means there would be ten absorption curves, making ten absorption curves closer by controlling L and C, finally get an broadband absorption[see Fig. 2(e)].

Different from the CNR metamaterial absorber, there is an opening structure in the nested rings of NROS metamaterial absorber, it means in each parallel LC resonant circuit, the inductance (*L*n, n=1, 2... 10) has been reduced [see Fig. 2(f)], while the equivalent circuit is a parallel circuit, the inductance (*L*) would be increased. The inductance (*L*) could be calculated as Eq.10:

$$\frac{1}{L} = \frac{1}{L_1} + \frac{1}{L_2} + \frac{1}{L_3} + \cdots + \frac{1}{L_{10}} \tag{10}$$

The inductance (*L*) has been reduced [see Fig. 2(f)], while the period of oscillation *T* is in direct proportion to inductance (*L*) [see Eq. 9], T of NROS absorber is longer than CNR absorber, it leads the broadband of NROS absorber is longer than it of CNR absorber [see Fig. 2(e)].

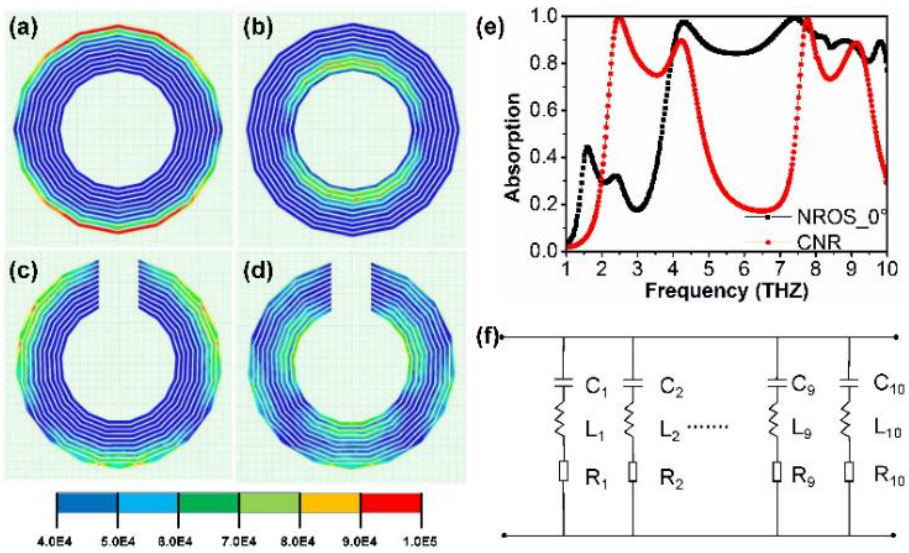

Fig. 2. (a) The current field distribution of the CNR metamaterial absorber at the resonance frequency 2.5 THZ. (b) The current field distribution of the CNR metamaterial absorber at the resonance frequency 4.3 THZ. (c) The current field distribution of the NROS metamaterial absorber at the resonance frequency 4.3 THZ. (d) The current field distribution of the NROS metamaterial absorber at the resonance frequency 7.2 THZ. (e) Absorption curves with optimized structural parameters of NROS absorber and CNR absorber. (f) Equivalent circuit diagram of CNR and NROS metamaterial absorber.

As Fig. 2(a-d) shown, the current field of the CNR metamaterial absorber at the resonance frequency (2.5 THZ and 4.3 THZ) is stronger than the NROS metamaterial absorber (4.3 THZ and 7.2 THZ). In LC resonance circuit, when the electric current has been increased, the oscillation period will be decreased. As Fig. 2(a-d) shown the current fields of the CNR metamaterial absorber at its resonance frequency are stronger than NROS metamaterial absorber, it means the oscillation period of the NROS metamaterial absorber is longer than CNR metamaterial absorber, it also proved that the broadband of NROS absorber is longer than CNR absorber.

3. Results and discussion

Following, we have defined the angle between the open structure and the positive direction of the magnetic field as α, which represents the angle between the positive direction of the magnetic field and the positive direction of central axis of opening structure [Fig. 3(a)]. Both parameters of α and d are proven to have highly effect on the absorption feature of the absorber.

As *d* increases from 1 to 6μm, the third absorption peak (arrow in Fig. 3(b)) shifts to the high frequency gradually, resulting in decreasing of bandwidth in the 4-8 THz. Otherwise, the absorption is below 80% in the 4-8 THz as the *d* is set as 1μm, while it below 80% in the 9-10 THz if *d* is set as 6μm [Fig. 3(b)]. As a result, *d* is optimized to be 5μm in our design. Fig. 3(c, d) plot absorption curves with various values of the α in the range of 0-90° at a step of 10°, respectively. The curve shape exhibits two obvious stages [Fig. 3(c, d)]. As α increases from 0 to 40°, the absorption gradually reduces to below 80% in 5-8 THz, but still above 60% [Fig. 3(c)]. In contrast, as α increases from 50° to 90°, the absorption broadband shifts to 2-5 THz, but the absorption increases in 2.5-3.5 THz [Fig. 3(d)]. In this regime, the smallest absorption is still above 70% (3.23 THz, α=50°), and the absorption broadband is calculated to be 2.8 THz (2.32-5.12 THz) at absorption above 70%. Finally, two isolated absorption broadband can be achieved when α are set to 0° and 50°, respectively, and the absorption bandwidth can be increased to 7.64THz (2.34-9.98 THz) by controlling the α.

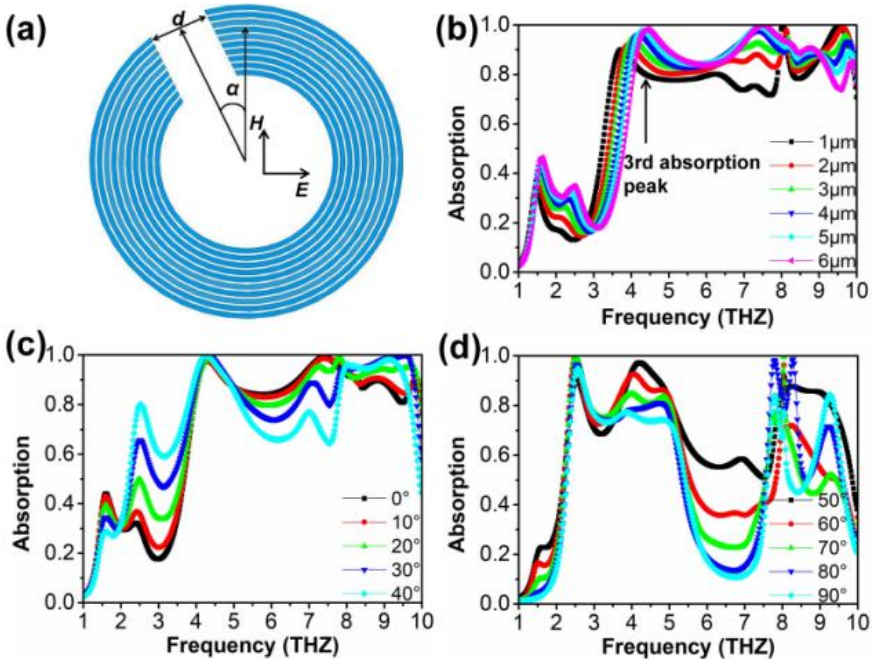

Fig. 3 (a) Schematic diagram of the NROS absorbing structure. (b) Absorption curves of NROS absorber with various *d*. Absorption curves of NROS absorber as α is set from 0° to 40° (c), and from 50° to 90° (d). All the absorption results are simulated by the TE polarization mode.

Furthermore, the structural parameters are systematically investigated by simulations. As the thickness of top layer (l_1) increases from 0.02 to 0.10 μm, the absorption curves keep the

similar shape but a little decrease of intensity in the 4-10 THz [Fig. 4(a)]. It indicates a little influence of the thickness of top metals. Therefore, the thickness of top metallic layer is set to 0.02μm in consideration of the convenience of fabrication process. For the middle dielectric layer, the absorption curves exhibit a big change at the different thicknesses (l_2) [Fig. 4(b)]. In brief, the absorption is below 80% in 5-7 THz as l_2<7μm, while a smaller value is found in 9-10 THz as l_2>7μm [Fig. 4(b)]. Therefore, l_2 is optimized to be 7 μm in our design.

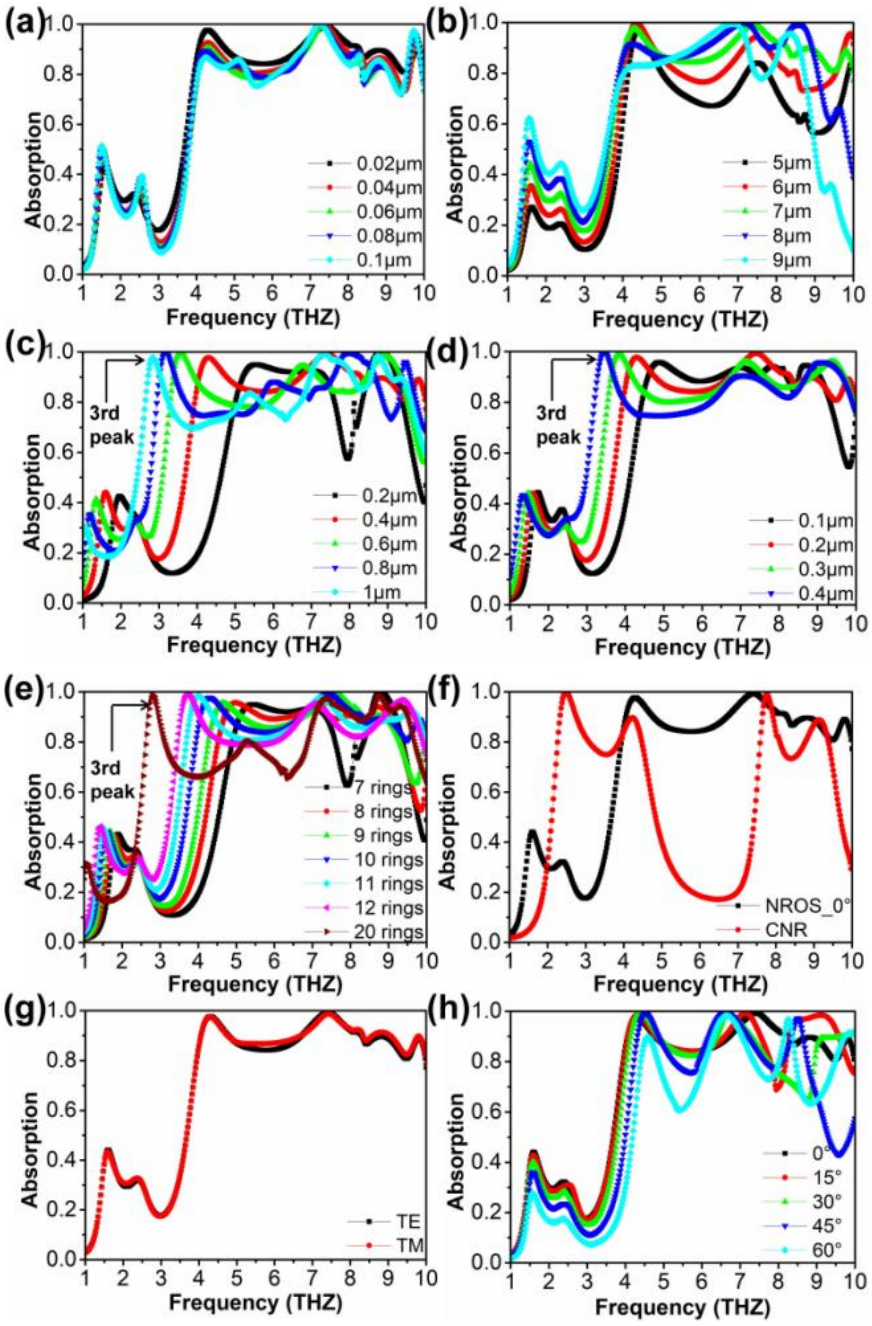

Fig. 4. (a) Thickness of top metallic layer (l_1). (b) Thickness of middle dielectric layer (l_2). (c) Width of metallic ring (x_3). (d) Distance of adjacent rings (x_4). (e) Number of metallic rings. (f) Absorption curves with optimized structural parameters of NROS

absorber and its controlled CNR absorber. (g) Absorption curves with different polarized incidence (TE and TM). (h) Absorption curves at polarization angles φ=0-60° at a step of 15°. All the absorption results are simulated by the TE polarization mode except Fig. 4(g).

For the width of each ring (x_3), it has a significant influence on the third absorption peak. As x_3 increases from 0.2 to 1.0 μm, the peak shifts to the lower frequency, which can extend absorption broadband efficiently [Fig. 4(c)]. However, there is part of absorption broadband between the third and fourth peak below 80% [Fig. 4(c)] as x_3>0.4μm. Meanwhile, there is still a part (7.5-8.5 THz) with absorption below 80% as x_3=0.2μm. Above all, x_3 is optimized to be 0.4μm herein. In addition, the distance between the adjacent rings (x_4) shows a remarkable influence on the absorption peak position and intensity. Fig. 4(d) shows a down shift of the third peak as increase of x_4, leading to extend of absorption regime. Meanwhile, the absorption intensity between the third and fourth peak gradually reduces, even below 80%. For additional reason, there is much difficult and high-cost in fabrication process if narrows the adjacent distance further. Above all, the x_4 was set to be 0.2 μm finally.

For the number of rings, the absorption curves [Fig. 4(e)] show a similar behavior as those of parameter of x_4. The third peak shifts to the low frequency as increase of number from 7 to 20, thereby extending the absorption broadband efficiently. However, the absorption intensity between the third and fourth peaks gradually decreases to below 80% if the number surpasses 10. To realize the ultra-broadband and reduce the complex of fabrication process, the number of metallic rings is set to 10 in our design.

After optimization analysis, the absorption bandwidth is kept about 6 THz when the diameter of the innermost (x_1) is about 14.4μm. Therefore, the x_1 is set to be 14.4 μm in our design. According to the optimized values of x_3, x_4 and number of rings, the diameter of the outmost circle (x_2) is calculated to be 26 μm. In addition, the absorption bandwidth has been kept about 6 THz when the periodicity (p) is around 30.

After optimization of structural parameters of absorber, a broadband of 6.04 THz at high frequency of 3.94-9.98 THz is achieved at incident angle of 0° [Fig. 4(f) black line]. Notably, all the absorption in this regime is above 80%, with the highest and average absorption of

99.26% and 89.43%, respectively. In contrast, a controlled absorber is developed which has the same structural parameters as the NROS absorber, but with 10 closed nested rings. It is named as "CNR". The red line in Fig. 4(f) exhibits its absorption curve. The absorption bandwidth is obtained cover two frequency regimes of 2.41 THz (from 2.23-4.64 THz) and 1.89 THz (from 7.52-9.41 THz). Nevertheless, the absorption bandwidth is narrower than that of "NROS" absorber, and the absorption is lower than 80% in most of absorption bandwidth too.

Fig. 4(g) plots absorption curves in the range of 1-10 THz at TM and TE polarized incidence. Two curves are near overlapped, indicating the proposed absorber is insensitive to the TM and TE polarization. The absorption band covers from 3.94 to 9.98 THz at the absorption above 80%. This broadband of 6.04THz at high frequency is rarely achieved before both in the simulation and experiment. Fig. 4(h) depicts the absorption curves with various incident angles of 0-60º at a step of 15º. Generally, the absorption curves show the similar shape with gradually decrease of intensity [Fig. 4(h)]. The largest bandwidth is calculated to be 6.23 THz at absorption above 60% achieved at β=0º, while it reduces to its smallest value of 5.05 THz at β=45º. The drop ratio is only 19%, suggesting the proposed NROS absorber is a terahertz polarization insensitive absorber.

Fig. 5 depicts the simulated 2D patterns of the electric field distribution of the NROS and CNR absorber at different absorption peaks. Fig. 5(a-c) depict the distribution of electric field at absorption peaks of 4.3, 7.2 and 8.8 THz, respectively, when the incident angle is 0º. The position of the maximum intensity moves from outer to inner ring, and back to outer one again. Meanwhile, the maximum electric field intensity gradually decreases [Fig. 5(a-c)], and the stronger field are mainly distributed near the opening structure [Fig. 5(a-c)]. When the incident angle is set to 70º, the absorption peak shifts to the high frequency and the distribution of electric field moves from outer ring to the inner one [Fig. 5(d-f)]. In addition, the distribution exhibits symmetrical about the central axis of the opening structure at three absorption peaks of 2.5, 4 and 5 THz, and the stronger field are mainly distributed near the opening structure too [Fig. 5(d-f)]. As a controlled experiment, the same simulations have been carried out on the CNR absorbers to investigate the distribution of electric field. Fig. 5(g-i) exhibit the field moves from

outer ring to inner one, and then back to outer one again. Meanwhile, the intensity of the electric field is gradually reduced.

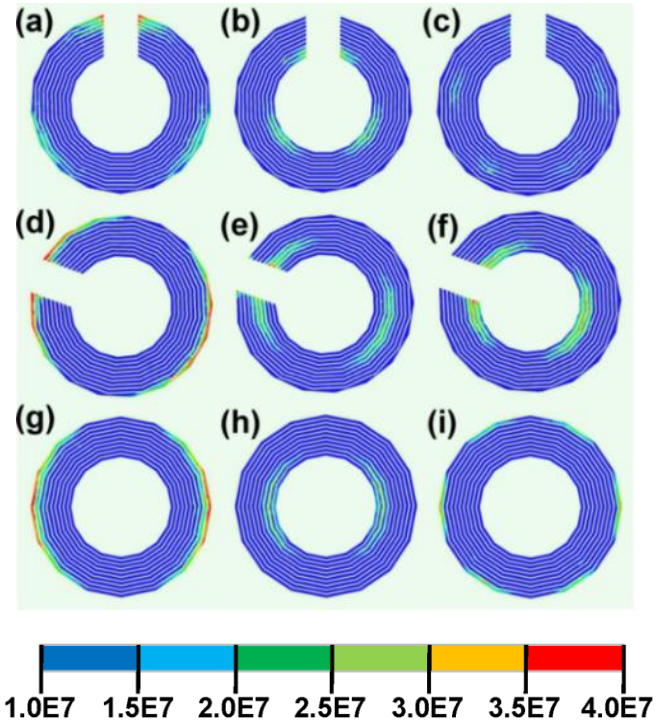

Fig. 5. 2D pattern of distribution of electric field at different absorption peaks. (a-c) The absorption peaks at 4.3, 7.2, 8.8 THz at α=0°, respectively. (d-f) The absorption peaks at 2.5, 4.0, 4.8 THz at α=70°, respectively. (g-i) The absorption peaks at 2.4, 4.3, 7.7 THz of CNR absorber, respectively.

Above all, three results can be drawn: 1) the strongest intensity of electric field mainly distributed near the opening structure; 2) the opening structure is response for the absorption peak in NROS absorber, which can also change the distribution of electric field compared to the CNR absorber; 3) the distribution of electric field is symmetrical about the central axis of opening structure. In the proposed structure, the periodic metallic layer is equivalent to an LC (inductance and capacitance) resonance circuit. In this circuit, the intensity of the electric field and the oscillation period (distance between two absorption peaks) are negatively correlated. As a result, the intensity of the electric field of CNR absorber is stronger than that of NROS one [see Fig. 5(g) and Fig. 5(a)], which means the oscillation period of CNR absorber is shorter than that of NROS one. With the reduced oscillation period, the distance between two closed absorption peaks will reduce, thereby the absorption broadband reduces accordingly.

Table 2 summarized our findings with the previous results. Significantly, the proposed NROS absorber shows the largest broadband at high terahertz frequency simultaneously. Bandwidth (BW) and Relative absorption bandwidth (RBW) are two important evaluation indexes of the THZ absorber. Compared with the previous results, our designed broadband absorber can cover almost all the high terahertz frequency. This high frequency (equal to short wavelength) absorber can be applied in tiny targets nondestructive detecting and accurate imaging. Meanwhile, the ultra-broadband of 6.04 THz may be used for radar monitoring and terahertz communication.

Table2. Design parameters of proposed absorber

Absorption	BW(THz)	RBW(THz)	Reference
>80%	1.85-2.48	29%	12
>80%	1.56-2.24	36%	13
>80%	1.30-3.00	79%	20
>80%	2.60-7.80	100%	25
>80%	2.60-7.80	100%	25
>80%	0.98-3.53	113%	26
>80%	1.23-1.68	62%	27
>80%	2.34-9.98	124%	Our work

4. Conclusion

In conclusion, we present an ultra-broadband terahertz absorber at high terahertz frequency. The absorption bandwidth is up to 6.04 THZ (3.94-9.98 THZ) at the absorption above 80%, while a near entire terahertz regime is achieved at the absorption above 60%. Meanwhile, the highest absorption is up to 99.26%, and the average value is still as high as 89.43%. In addition, the proposed absorber exhibits insensitive to the TM and TE polarization no matter what kinds of incident angles are applied. The opening structure is response for such a wide absorption broadband, and the absorption broadband can be regulated by adjusting the incident angle.

Acknowledgements

This work was supported by the National Key R&D Program of China (Grant No. 2019YFA0705201), National Natural Science Foundation of China (Grant No. 61771156), Foundation for Innovative Research Groups of the National Natural Science Foundation of China (Grant No.51521003), Project funded by China Postdoctoral Science Foundation (CA24407217).

References.

1. P. H. Siegel "Terahertz technology," IEEE Transactions on Microwave Theory and Techniques, vol. 50, no. 3, pp. 910-928,2002.
2. T. J. Yen, W. J. Padilla, N. Fang, D. C. Vier, D. R. Smith, J. B. Pendry, D. N. Basov, and X. Zhang, "Terahertz magnetic response from artificial materials," Science, vol. 303, no. 5663, pp. 1494-1496, 2004.
3. Z. Y. Song, K. Wang, J. W. Li, and Q. H. Li, "Broadband tunable terahertz absorber based on vanadium dioxide metamaterials," Optics Express, vol. 26, no. 6, pp. 7148-7152, 2018.
4. Y. N. Jiang, H. D. Zhang, J. Wang, C. N. Gao, J. Wang, and W. P. Cao, "Design and performance of a terahertz absorber based on patterned graphene," Optics Letters, vol. 43, no. 17, pp. 4296-4299, 2018.
5. P. Pitchappa, C.P. Ho, L. Cong, R. Singh, N. Singh, and C. Lee, "Reconfigurable digital metamaterial for dynamic switching ofterahertz anisotropy," Advanced Optical Materials, vol. 4, no. 3, pp. 391-398, 2016.
6. Z. Song, A. Chen, and J. Zhang, "Terahertz switching between broadband absorption and narrowband absorption," Optics Express, vol. 28, no. 2, pp. 2037-2044, 2020.
7. J. W. Chen, J. D. Hu, X. H. Deng, and J. R. Yuan, "Enhanced THz absorption of graphene cavity-based electromagnetic metamaterial structures," Journal of Modern Optics, vol. 67, no. 6, pp. 547-551, 2020.
8. I. S. Abramov, E. D. Gospodchikov, A. G. Shalashov. "Extreme Ultraviolet Radiation Source Based on a Discharge Sustained by a Radiation Pulse from a Terahertz Free-Electron Laser," Journal of Experimental and Theoretical Physics, vol. 132, no. 2: 223-232, 2021.
9. X. Z. Chen, X. Liu, X. D. Guo, S. Chen, H. Hu, E. Nikulina, X. L. Ye, Z. H. Yao, H. A. Bechtel, M. C. Martin, G. L. Carr, Q. Dai, S. L. Zhuang, Q. Hu, Y. M. Zhu, R. Hillenbrand, M. K. Liu, and G. J. You, "THz near-field imaging of extreme subwavelength metal structures," ACS Photonics, vol. 7, no. 3, pp. 687-694, 2020.
10. N. I. Landy, S. Sajuyigbe, J.J. Mock, D.R. Smith, and W.J. Padilla, "Perfect metamaterial absorber," Physical review letters, vol. 100, no. 20, pp. 207402-207408, 2008.
11. T. Wu, Y. Shao, S. Ma, G. Wang, and Y. Gao. "Broadband terahertz absorber with tunable frequency and bandwidth by using dirac semimetal and strontium titanate," Optics Express, vol. 29, no. 5, pp. 7458-7467, 2021.
12. M. Biabanifard, A. Arsanjani, M. S. Abrishamian and D. Abbott, "Tunable terahertz graphene-based absorber design method based on a circuit model approach," IEEE Access, vol. 8, no. 99, pp. 70343-70354, 2020.
13. J. J. Bai, M. L. Ge, J. N. Li, C. X. Tang, X. D. Sun, H. Y. Xing, and S. J. Chang, "Numerical investigation of broadband THz metamaterial absorber with double composite structure layer," Optics Communications, vol. 423, no. 15, pp. 63-68, 2018.
14. Y. Ma, Q. Chen, J. Grant, S. C. Saha, A. Khalid, and D. R. S. Cumming, "Polarisation insensitive, broadband THz metamaterial absorber," Optics Letters, vol. 36, no. 17, pp. 3476-3478, 2011.
15. K. D. Xu, J. Li, A. X. Zhang, and Q. Chen, "Tunable multi-band terahertz absorber using single-layer square graphene ring structure with T-shaped graphene strips," Optics Express, vol. 28, no. 8, pp. 11482-11492, 2020.
16. J. Huang, J. Li, Y. Yang, J. Li, J. H. Li, Y. Zhang, and J. Q. Yao, "Active controllable dual broadband terahertz absorber based on hybrid metamaterials with vanadium dioxide," Optics Express, vol. 28, no. 5, pp. 7018-7027, 2020.

17. V. K. Verma, S. K. Mishra, K. K. Kaushal, V. Lekshmi, S. Sudhakar, N. Gupta, and B. Appasani, "An octaband polarization insensitive terahertz metamaterial absorber using orthogonal elliptical ring resonators," Plasmonics, vol. 15, no. 1, pp. 75-81, 2020.

18. B. X. Wang, Y. H. He, N. X. Xu. X. Y. Wang, and Y. C. Wang, "Design of dual-band polarization controllable metamaterial absorber at terahertz frequency," Results in Physics, vol. 17, pp. 103077-103079, 2020.

19. Z. Huang, H. Chen, Y. Huang, Z. Ge, Y. Zhou, Y. Yang, P. S. Xiao, J. J Liang, T. F. Zhang, Q. Shi, G. H. Li, and Y. S. Chen, "Ultra-broadband wide-angle terahertz absorption properties of 3D graphene foam," Advanced Functional Materials, vol.28, no. 2, pp. 1704363-1704371, 2018.

20. D. Y. Zhu, Y. Wang, L. P. Song, and Z. J. Cui, "Semiconductor-based broadband absorber in terahertz band," Ferroelectrics, vol. 549, no. 1, pp. 104-110, 2019.

21. B. X. Wang, L. L. Wang, G. Z. Wang, W. Q. Huang, X. F. Li, and X. Zhai, "Theoretical investigation of broadband and wide-angle terahertz metamaterial absorber," IEEE Photonics Technology Letters, vol. 26, no. 2, pp. 111-114, 2014.

22. Z. Liu, L. Guo, and Q. Zhang, "A simple and efficient method for designing broadband terahertz absorber based on singular graphene metasurface," Nanomaterials, vol. 9, no. 10, pp. 1351-1355, 2019.

23. O. M. Daraei, K. Goudarzi, and M. Bemani, "A tunable ultra-broadband terahertz absorber based on two layers of graphene ribbons," Optics & Laser Technology, vol. 122, pp.105853-105857, 2020.

24. S. Mohamadreza, N. Alireza, C. Iman, and B. Sadegh, "A configurable two-layer four-bias graphene-based THz absorber," Journal of Computational Electronics, 2020: 1-17., vol. 19, no. 1, pp. 719-735, 2018.

25. J. Lv, R. Y. Yuan, X. Song, and H. Yan, "Broadband polarization-insensitive terahertz absorber based on heavily doped silicon surface relief structures" Journal of Applied Physics, vol. 117, no. 1, pp. 013101-013104, 2015.

26. Y. H. Wu, Y. Q. Deng, J. J. Wang, Z. Y. Zong, X. Chen, and W. H. Gu, "THZ broadband absorber fabricated by EHD-printing technology with high error tolerance", IEEE Transactions on Terahertz Science and Technology, vol. 9, no. 6, pp. 637-642, 2019.

27. H. Feng, Z. Xu, L. I. Kai, M. Wang, and M. Yun, "Tunable polarization-independent and angle-insensitive broadband terahertz absorber with graphene metamaterials," Optics Express, vol. 29, no. 5, pp. 7158-7167, 2021.